Oil Shale, 2025, Vol. 42, No. 1, pp. 29–61
doi: https://doi.org/10.3176/oil.2025.1.02
ISSN 0208-189X

Geochemistry of the coal-bearing member of the Middle Jurassic Shimengou Formation, Tuanyushan area of the Qaidam Basin, NW China: implications for the formation of oil shale

Yinbo Xu[a,b], Shi Fang[a]*, Shuqing Yao[c], Pingchang Sun[a], Caiqin Bi[b], Yaohua Li[b], Weibin Liu[b], Kun Yuan[b], Peizhen Zhang[d]

[a] College of Earth Sciences, Jilin University, Changchun, Jilin 130061, China
[b] Oil and Gas Survey, China Geological Survey, Beijing 100083, China
[c] Geoscience Documentation Center, China Geological Survey, Beijing 100083, China
[d] School of Earth Sciences and Engineering, Sun Yat-Sen University, Guangzhou, Guangdong 510275, China

Received 14 June 2024, accepted 10 January 2025, available online 14 January 2025

Abstract. *Abundant coal and oil shale resources are developed in the coal-bearing member of the Shimengou Formation (J_2sh^1) in the northern Qaidam Basin, NW China. A better understanding of the formation mechanism of these oil shales is of great significance for the exploration of potential unconventional oil and gas resources, and the co-development of coal and oil shale resources. In this study, the geochemistry of 16 samples from drilling cores was used to determine paleoclimate, paleosalinity, redox conditions, chemical weathering intensity, provenance, and tectonic setting. The results show that the geochemical characteristics of the samples are similar to the composition of the upper continental crust, with a warm and humid paleoclimate, a freshwater to brackish paleosalinity condition, a generally anoxic condition, and intense weathering during the Middle Jurassic. The provenance was mainly felsic igneous rocks, and the prevailing tectonic setting was passive margin. During the Middle Jurassic, the warm and humid climate, caused by the low paleolatitude and water vapor from the Tethys Ocean, made the provenance mainly from Hercynian intrusive rocks, which underwent intense weathering and entered the northern Qaidam Basin along with plant material. During water regression periods, abundant terrestrial plants formed coal, while during flooding periods, the increasing water depth and the input of nutrients from terrestrial debris promoted the development of lake algae. Algae and other lake organisms, as well as terrestrial plants, provided the material basis for the formation of organic matter. The anoxic preservation conditions enabled the preservation of organic matter, resulting in the formation of oil shale. This study helps to understand the formation mechanism of the J_2sh^1 oil shale and promotes the utilization of oil shale in the studied area.*

* Corresponding author, fs812625@vip.sina.com

Keywords: *chemical index of alteration, provenance, tectonic setting, paleoenvironment, metallogenic model, Qaidam Basin.*

1. Introduction

The Qaidam Basin is an important continental oil and gas basin in northwestern China, where petroleum, natural gas, shale gas, and shale oil are developed [1–5]. Additionally, oil shale and coal are significant energy sources in the Qaidam Basin [6]. These two types of energy resources are found in the Middle Jurassic Shimengou Formation, with especially abundant deposits in the Shimengou Formation (Fm; J_2sh). This formation consists of the lower coal-bearing member (J_2sh^1) and the upper shale member (J_2sh^2), the latter of which features oil shale of much better quality and greater thickness, and has thus been the focus of previous studies [6, 7]. However, recent studies show that oil shale in J_2sh^1 is also well-developed and coexists with coal [8]. The joint exploitation and development of oil shale and coal can reduce production costs and increase profits, as in the case of the Fushun oil shale mine. This mine is China's most important oil shale production base, accounting for about 50% of the country's total oil production from oil shale [9]. Therefore, studying the oil shale and coal in J_2sh^1 is highly significant. This study helps to promote the development of oil shale in the Qaidam Basin.

Previous studies show that the material composition of rocks determines their geochemical characteristics [10]. The components of sedimentary rocks originate from source rocks, and thus the chemical characteristics of sedimentary rocks are mainly controlled by source rocks [11]. In addition, the components and chemical characteristics of sedimentary rocks are affected by paleoenvironment, paleowater conditions, and weathering conditions [11, 12]. Therefore, extensive studies have been conducted on the enrichment and distribution characteristics of major, trace, and rare earth elements (REE) in mudstone to investigate the provenance, weathering conditions, tectonic settings, and paleoenvironment [13].

Research on the provenance, weathering conditions, and tectonic setting of the sedimentary rocks in the Qaidam Basin has mainly focused on Cenozoic strata due to their significance in understanding the tectonic evolution of the Qinghai–Tibet Plateau [14–20]. Furthermore, Shu et al. [21] and Zhao et al. [22] carried out provenance studies of the entire Jurassic strata based on the detrital zircon geochronology. Yuan et al. [23] investigated the provenance of Early–Middle Jurassic strata based on zircon U–Pb ages. Zhang et al. [19] studied the geochemical characteristics, provenance, and paleodepositional environments of the Lower Jurassic Huxishan Fm [24].

However, the provenance, source weathering, tectonic setting, and paleoenvironmental conditions of the Middle Jurassic Shimengou Fm remain insufficiently studied. Most previous studies have focused on the metallogenic

conditions, quality characteristics, and distribution of the J_2sh^2 oil shale [6, 7]. Due to the differences between the J_2sh^2 and J_2sh^1 oil shales, existing studies are inadequate for understanding the formation mechanisms of the J_2sh^1 oil shale. Further research is needed on the J_2sh^1 oil shale associated with coal, especially regarding the controlling factors of provenance, source weathering, tectonic settings, and paleoenvironmental conditions.

2. Geological setting

The Qaidam Basin is located in northwestern China, in the northeastern part of the Qinghai–Tibet Plateau, and belongs to the eastern part of the Tethys tectonic domain (Fig. 1a, b) [25, 26]. It is surrounded by the eastern Kunlun Mountains in the south, the Qilian Mountains in the east, and the Altyn-Tagh Range in the northwest. The basin extends 850 km from east to west and 350 km from north to south, covering an area of about 120,000 km^2 [22, 27] (Fig. 1c). The Qaidam Basin consists of four primary structural units: the northern Qaidam Basin, the Yiliping Depression, the Sanhu Depression, and the West Qaidam Uplift (Fig. 1c) [27].

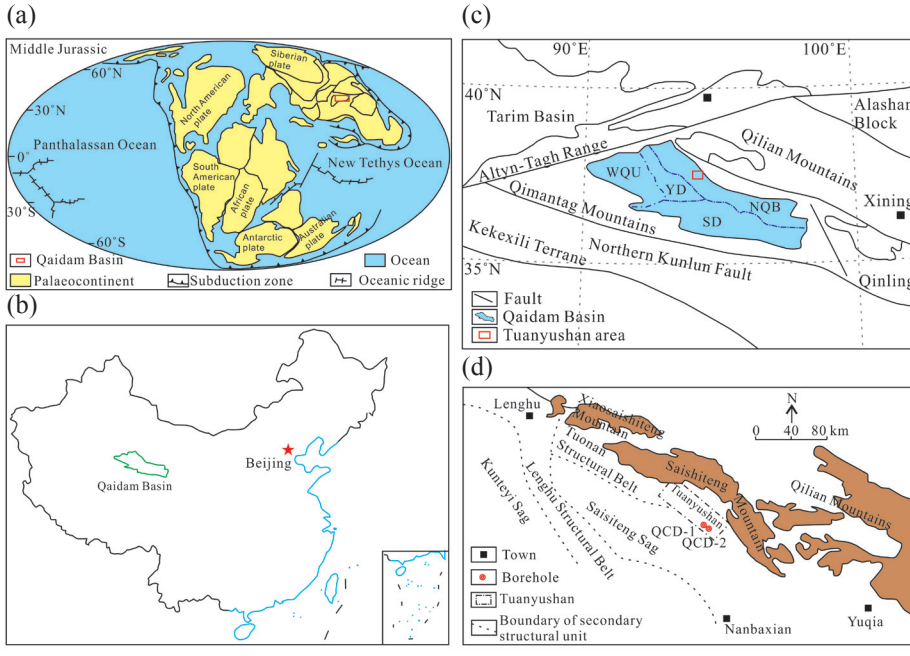

Fig. 1. (a) Middle Jurassic paleogeographic location of the Qaidam Basin (modified from [29]); (b) schematic map showing the location of the Qaidam Basin in China; (c) present-day location and tectonic setting of the Qaidam Basin [8]; (d) geological setting of the northern Qaidam Basin, including the study area and the QCD-1 and QCD-2 sampling wells [8]. Abbreviations: NQB – northern Qaidam Basin, YD – Yiliping Depression, SD – Sanhu Depression, WQU – West Qaidam Uplift.

The Qaidam Block was combined with its surrounding tectonic units, including the Qilian orogenic belt, the eastern Kunlun tectonic belt, and other adjacent blocks, after the Early Paleozoic Caledonian and Indosinian collision orogenies [22]. It developed into a Meso-Cenozoic intra-continental basin during the Late Triassic tectonic movements [22]. After accumulating Jurassic and Early Cretaceous deposits, the Qaidam Basin was uplifted and modified during the Late Cretaceous [28]. Extensive Cenozoic strata subsequently deposited in the basin due to the Indo-Eurasian plate convergence and collision [22]. Furthermore, the Jurassic strata underwent multistage tectonic uplift and deformation events between the Late Eocene and the Late Pliocene [28], leading to the current distribution pattern of these strata.

The Qaidam Basin is an important large Meso-Cenozoic petroliferous basin in China. Its stratigraphy consists of a basement of Presinian crystalline rocks and Sinian to Triassic non-metamorphic or low-grade metamorphic rocks, and a sedimentary unit of Mesozoic (Jurassic and Lower Cretaceous sediments) and Cenozoic strata [30]. The coal-bearing strata and lacustrine mudstones of the Lower to Middle Jurassic are important source rocks in the Qaidam Basin [31]. The Lower Jurassic strata include the Huxishan and Xiaomeigou formations, which were mainly deposited in fluvial, deltaic, swamp, and lacustrine environments, with sediments mostly consisting of sandstone, mudstone, and coal beds [8, 16]. The Middle Jurassic strata includes the Dameigou and Shimengou formations, with similar sedimentary environments and sediments as those of the Lower Jurassic strata [16].

Wang et al. [8] found that braided river delta and lake sediments are the primary sediments observed in the cores of the QCD-1 and QCD-2 wells from the Shimengou Fm in the Tuanyushan study (Fig. 1d) [8]. J_2sh^1 was mainly deposited in lake and braided river delta environments, with the lake facies including shallow lake and swamp, and the braided river delta facies consisting of braided river delta front and braided river delta plain. J_2sh^2 was mostly deposited in lake environments, consisting of shallow lake and deep lake. According to previous studies, oil shale develops with coal in J_2sh^1 and independently in J_2sh^2 [8]. This contribution focuses on J_2sh^1 to analyze the metallogenic background of coal and oil shale based on geochemistry, as well as its indications of paleoenvironment, provenance, and tectonic setting.

3. Samples and methods

Sixteen samples were collected from the QCD-2 well in J_2sh^1 in the Tuanyushan area of the northern Qaidam Basin. Among them, six samples are oil shale, and the other ten are mudstone (Fig. 2). The oil shale samples are black, while the mudstones samples range from dark gray to black. The mudstone samples can be divided into three types: mudstone, organic-rich mudstone, and carbonaceous mudstone. The samples darken in color progressively from mudstone to carbonaceous shale.

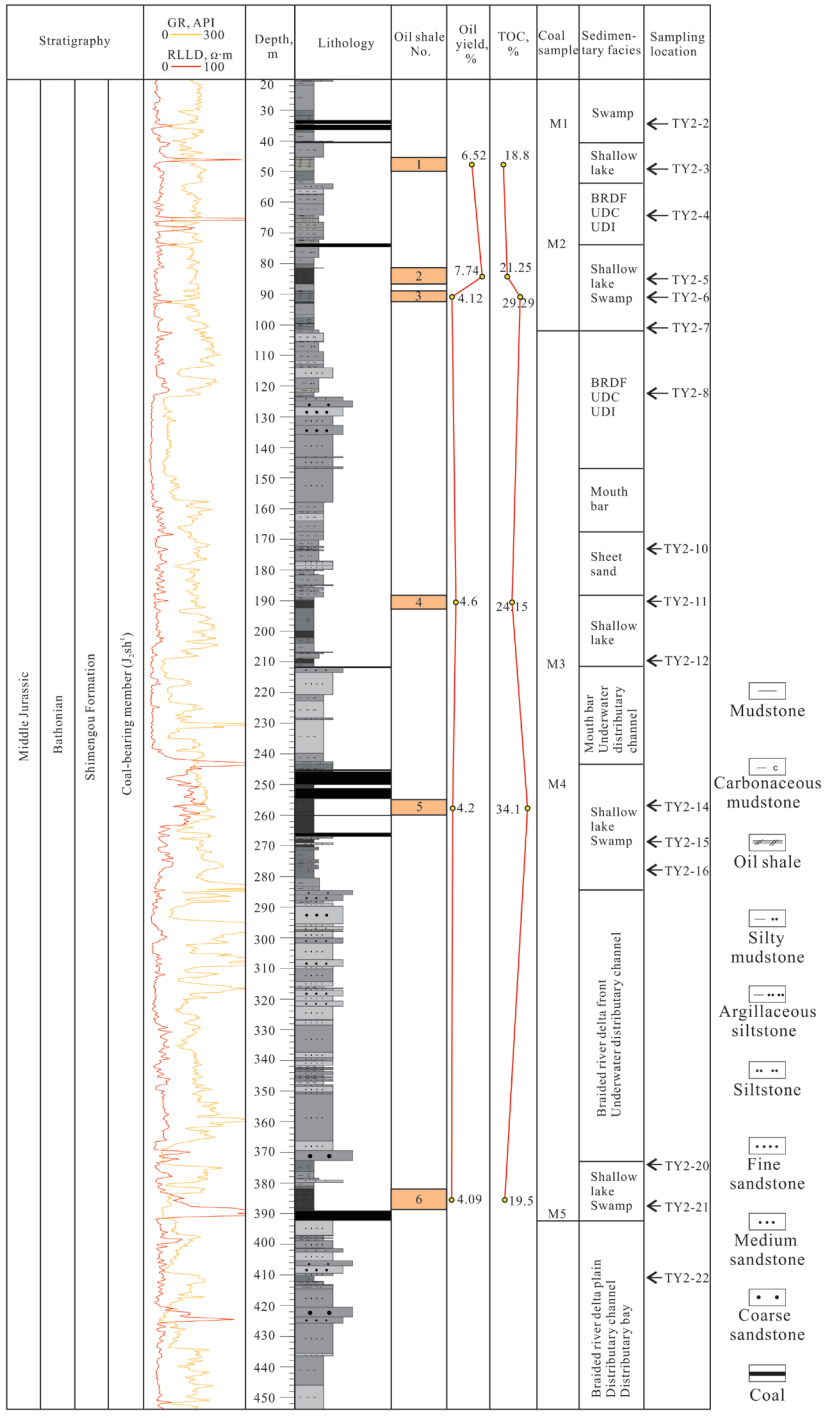

Fig. 2. Lithology and sampling points of the QCD-2 well (modified from [8]). Abbreviations: GR – natural gamma, RLLD – resistivity, BRDF – braided river delta front, UDC – underwater distributary channel, UDI – underwater distributary interchannel.

The samples were crushed to 200 mesh before testing and analysis. All 16 samples were analyzed for elemental concentrations by the Beijing Research Institute of Uranium Geology of the China National Nuclear Corporation. The major element contents were determined using a Philips PW2404 X-ray fluorescence (XRF) spectrometer, in accordance with the Chinese National Standard GB/T14506.28-2010, with an accuracy better than 2%. The analysis process was as follows: the powdered samples were heated to 1150 °C to form fused samples for XRF analysis after being mixed with lithium tetraborate, lithium fluoride, ammonium nitrate, and lithium bromide. The trace and rare earth element contents were determined using Element XR, in accordance with the Chinese National Standard GB/T14506.30-2010, with an accuracy better than 5%. The analysis process was as follows: the powder samples were dissolved with nitric acid, diluted for ICP-MS analysis after being dissolved in hydrofluoric and nitric acids in a closed dissolution chamber, and heated to remove remaining hydrofluoric acid.

4. Results

4.1. Total organic carbon and oil yield

The total organic carbon (TOC) contents of the studied samples vary between 1.10% and 34.10% (Table 1). Among these, six samples are classified as oil shale, with oil yields ranging from 4.09% to 7.74% and TOC values ranging from 19.5% to 34.1% (Fig. 2). The remaining samples are divided into three types of rocks based on TOC: mudstone (TOC <2%), organic-rich mudstone (TOC between 2% and 6%), and carbonaceous mudstone (TOC >6%). Overall, the samples exhibit high TOC contents.

4.2. Major elements

The major element contents (as oxides) of the J_2sh^1 samples are shown in Table 1, which demonstrates considerable variation. The analysis results reveal that SiO_2 and Al_2O_3 are the dominant components, with average concentrations exceeding 10%. SiO_2 contents range from 19.28% to 63.67%, with an average value of 41.48%, while Al_2O_3 contents range from 10.39% to 30.57%, with an average value of 21.49%. The average concentrations of TFe_2O_3 and K_2O fall between 1% and 2.5%, whereas the average concentrations of MgO, CaO, TiO_2, Na_2O, P_2O_5, and MnO are <1%.

The relationships between SiO_2 and other major elements show that K_2O and TiO_2 have a strong positive correlation with SiO_2, Al_2O_3 and MgO exhibit a medium positive correlation with SiO_2, while CaO shows a strong negative correlation with SiO_2, and Na_2O, TFe_2O_3, and P_2O_5 display no obvious correlation with SiO_2 (Fig. 3). The positive correlation between SiO_2, Al_2O_3, and K_2O suggests that silicon, aluminum, and potassium are mainly derived

Table 1. Major element concentrations of J_2sh^1 in the Tuanyushan area of the Qaidam Basin (%)

Sample	Lithology	TOC	SiO_2	Al_2O_3	TFe_2O_3	MgO	CaO	Na_2O	K_2O	MnO	TiO_2	P_2O_5	LOI	CIA*
TY2-2	Mudstone	29.29	32.67	16.89	1.15	0.6	0.54	0.23	1.23	0.004	0.57	0.07	43.87	90.72
TY2-3	Oil shale	18.80	46.24	22.01	1.86	0.74	0.37	0.2	2.26	0.004	0.69	0.08	24.97	88.78
TY2-4	Mudstone	4.35	24.39	10.39	5.76	8.82	18.74	0.07	1.16	0.073	0.45	0.31	29.51	87.66
TY2-5	Oil shale	21.25	36.52	16.41	1.74	0.49	1.17	0.22	1.40	0.006	0.64	0.74	40.08	88.20
TY2-6	Oil shale	29.29	19.92	11.28	2.09	0.41	1.96	0.23	0.80	0.006	0.32	0.17	62.33	89.35
TY2-7	Mudstone	1.10	57.29	25.40	1.73	0.80	0.31	0.19	2.75	0.007	0.85	0.15	9.93	88.39
TY2-8	Mudstone	6.90	49.83	22.61	3.13	0.79	0.38	0.17	2.27	0.007	0.86	0.10	19.28	89.09
TY2-10	Mudstone	5.00	53.9	23.65	3.75	0.93	0.37	0.19	2.51	0.078	0.86	0.10	13.25	88.55
TY2-11	Oil shale	24.15	18.92	11.58	2.19	0.48	1.66	0.23	1.20	0.006	0.42	0.17	62.83	86.71
TY2-12	Mudstone	11.70	43.78	24.14	3.00	0.84	0.55	0.24	2.12	0.01	0.65	0.12	24.33	89.84
TY2-14	Oil shale	34.10	42.54	29.33	0.91	0.21	0.37	0.19	0.86	0.004	0.88	0.17	24.07	95.60
TY2-15	Mudstone	3.69	44.65	29.77	1.04	0.25	0.33	0.13	1.14	0.005	0.90	0.17	21.04	95.03
TY2-16	Mudstone	3.87	42.58	28.83	1.12	0.25	0.33	0.13	1.21	0.004	0.77	0.12	24.28	94.79
TY2-20	Mudstone	2.15	44.96	30.57	0.90	0.21	0.33	0.12	1.07	0.004	1.04	0.32	19.99	95.33
TY2-21	Oil shale	19.50	19.28	12.13	1.66	0.20	0.81	0.32	0.33	0.014	0.41	0.13	63.45	92.67
TY2-22	Mudstone	1.57	63.67	19.00	1.24	0.61	0.21	0.14	2.57	0.007	0.83	0.05	11.12	86.41

* Chemical index of alteration. For the formula for calculating the CIA value [33], see Section 5.3.

from clay minerals. In addition, a strong positive correlation between TiO_2 and Al_2O_3 ($R^2 = 0.79$) indicates the presence of terrigenous substances in the samples [32].

4.3. Trace elements

The main trace element contents of the J_2sh^1 samples are listed in Table 2, and the distribution patterns of Post-Archean Australian shale (PAAS, [34])-normalized trace elements are presented in Figure 4a. Among these elements, Th and Y (high-field-strength elements), Ba and Sr (large-ion lithophile elements), and Zn (a transition trace element) are distinctly enriched. U (a high-field-strength element), Cu (a chalcophile and redox-sensitive element), and Mo (a transition trace element) are slightly enriched. Ni and Cr (transition trace elements), V and Rb (large-ion lithophile elements), and Zr (a high-field-strength element) are distinctly depleted, while Sc (a high-field-strength element) and Co (a transition trace element) are slightly depleted compared with the PAAS. The depletion of Sc, V, and Cr (ferriphilic magnesium elements) reflects a limited contribution from magnesite source rocks to the samples. Additionally, the differing distribution characteristics of Co, Ni, and Zn across various samples may indicate the presence of multiple provenance sources.

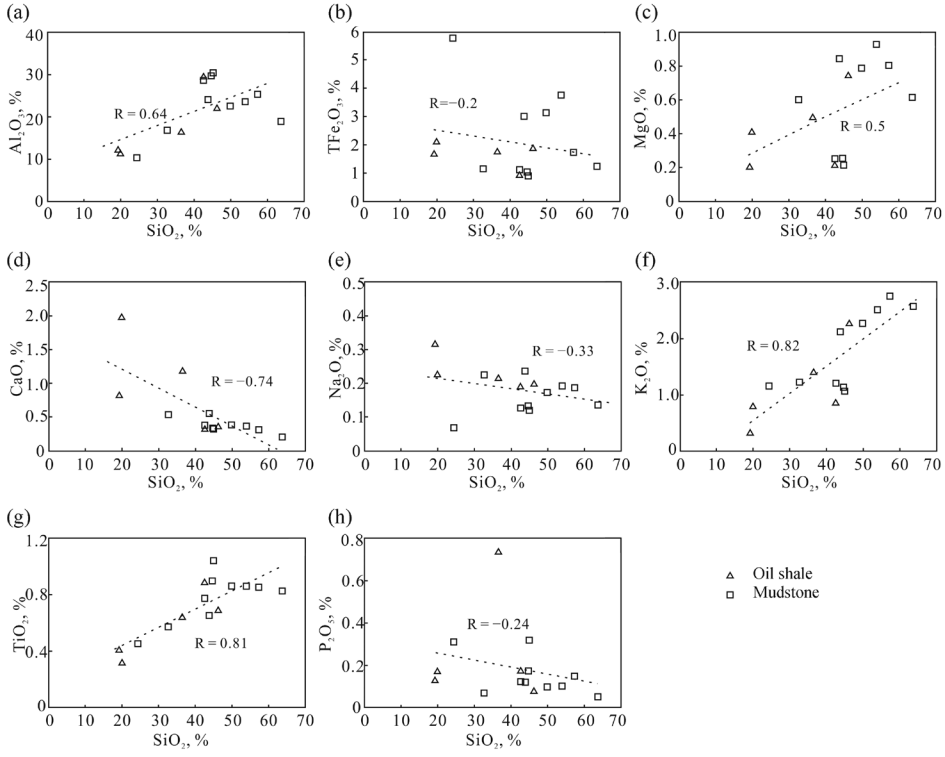

Fig. 3. Relationship between SiO_2 and other major elements.

Table 2. Trace element concentrations of J_2sh^1 in the Tuanyushan area of the Qaidam Basin (ppm)

Sample	Lithology	Sc	V	Cr	Co	Ni	Cu	Zn	Rb	Sr	Y	Mo	Ba	Th	U	Zr	Hf
TY2-2	Mudstone	9.86	70.80	47.00	3.36	15.00	46.00	40.70	93.10	196.00	25.90	1.04	6423.00	17.50	5.75	132.00	4.43
TY2-3	Oil shale	17.40	146.00	90.20	80.40	158.00	50.80	61.40	169.00	157.00	42.70	3.88	1088.00	32.50	10.90	235.00	6.50
TY2-4	Mudstone	8.37	46.00	39.10	4.42	21.60	17.70	38.30	67.60	92.80	24.80	0.24	388.00	15.10	3.36	140.00	4.08
TY2-5	Oil shale	18.70	127.00	73.70	12.70	35.50	105.00	142.00	95.70	369.00	97.40	2.96	1437.00	22.90	8.90	178.00	5.43
TY2-6	Oil shale	15.80	94.40	49.20	12.60	35.10	97.30	71.40	80.70	279.00	58.00	3.77	2243.00	18.20	8.05	103.00	3.13
TY2-7	Mudstone	15.70	89.30	70.80	6.05	27.70	23.20	69.20	176.00	257.00	36.20	0.68	701.00	26.60	5.89	177.00	5.35
TY2-8	Mudstone	18.30	108.00	76.90	26.80	37.80	87.80	115.00	135.00	139.00	49.30	1.05	424.00	28.90	5.24	228.00	6.96
TY2-10	Mudstone	19.50	118.00	78.60	88.70	124.00	34.80	107.00	146.00	119.00	48.50	3.05	432.00	26.40	5.96	204.00	6.04
TY2-11	Oil shale	14.72	101.42	54.52	23.11	50.34	70.02	217.34	87.06	255.20	53.50	4.29	1457	24.16	7.87	140.00	4.24
TY2-12	Mudstone	19.20	113.00	84.10	36.90	42.60	48.50	120.00	148.00	157.00	53.60	1.44	1045.00	29.50	5.32	166.00	4.81
TY2-14	Oil shale	13.20	86.70	31.90	5.80	12.40	18.10	769.00	68.40	220.00	40.90	4.51	379.00	27.70	7.25	129.00	4.25
TY2-15	Mudstone	16.40	71.50	33.10	6.25	11.50	23.40	105.00	66.90	279.00	57.10	4.10	1287.00	43.60	9.91	120.00	3.85
TY2-16	Mudstone	20.00	97.90	36.20	15.40	19.40	77.20	107.00	70.10	145.00	94.30	5.08	659.00	48.90	24.40	110.00	3.52
TY2-20	Mudstone	16.30	68.10	30.00	3.80	13.10	25.00	54.60	56.30	517.00	68.90	5.57	757.00	30.90	8.42	136.00	4.39
TY2-21	Oil shale	8.49	53.00	27.60	4.05	10.70	78.90	42.90	21.50	251.00	28.50	6.33	2139.00	19.50	4.24	55.30	1.88
TY2-22	Mudstone	15.20	74.90	65.90	9.55	16.70	25.90	92.60	149.00	87.30	34.30	0.82	506.00	21.50	6.93	358.00	10.40
PAAS*		16.0	150	110	23	55	50	85	160	200	27	1.00	650	15.00	3.10	210	5.00

* PAAS data from [34].

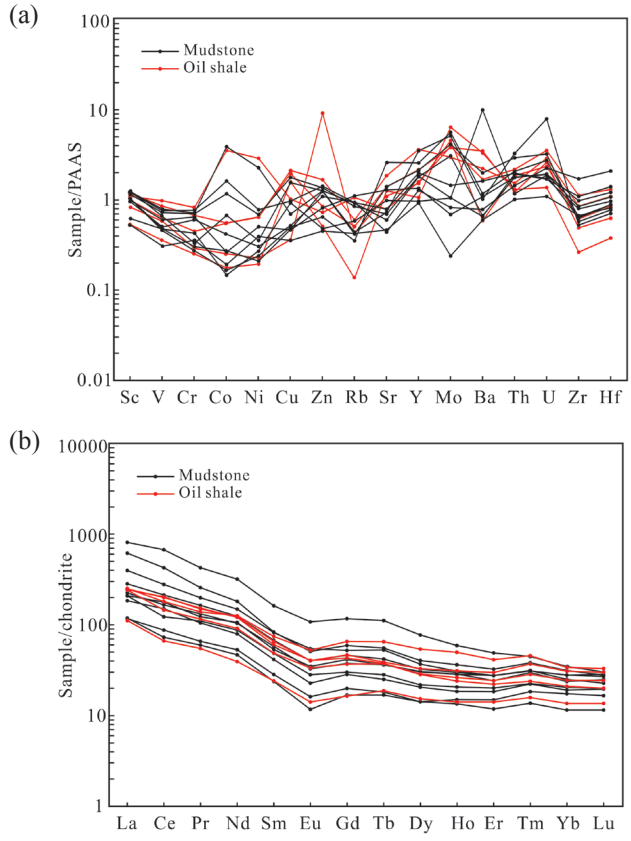

Fig. 4. (a) PAAS-normalized trace element diagram and (b) chondrite-normalized rare earth element diagram for samples from the coal-bearing member of the Shimengou Formation in the Tuanyushan area (PAAS data from [34]; chondrite data from [35]).

4.4. Rare earth elements

The REE contents of the J_2sh^1 samples are presented in Table 3. The total REE concentrations (ΣREE) vary greatly from 142.19 to 1163.75 ppm, with an average of 395.03 ppm, which is significantly higher than those of the North American shale component (NASC, 173.41 ppm) [36]. The concentrations of light REEs (ΣLREE) are significantly higher than those of heavy REEs (ΣHREE), with ΣLREE/ΣHREE ratios ranging from 5.66 to 14.21, averaging 9.08. The δCe values range from 0.81 to 1.14, with an average value of 0.99, indicating a slight negative anomaly. The δEu values vary from 0.58 to 0.83, with an average value of 0.73, showing an obvious negative anomaly. Additionally, the samples are characterized by enrichment in LREEs and depletion in HREEs (Fig. 4b). These characteristics may indicate that the provenance is mainly from the upper continental crust (Table 3).

Table 3. Rare earth element concentrations of J_2sh^1 in the Tuanyushan area of the Qaidam Basin (ppm)

Sample	Lithology	La	Ce	Pr	Nd	Sm	Eu	Gd	Tb	Dy	Ho	Er	Tm	Yb	Lu	∑REE	∑LREE/ ∑HREE	δEu	δCe
TY2-2	Mudstone	36.90	59.00	7.16	28.00	4.76	0.82	4.39	0.84	4.54	1.05	3.12	0.55	3.65	0.50	155.28	7.33	0.58	0.86
TY2-3	Oil shale	77.00	162.00	18.30	72.60	12.10	2.84	11.20	1.88	9.20	1.84	5.12	0.85	5.14	0.73	380.80	9.59	0.79	1.03
TY2-4	Mudstone	36.30	70.90	7.90	31.90	5.68	1.13	5.17	0.91	4.53	0.94	2.48	0.41	2.42	0.35	171.02	8.94	0.68	1.00
TY2-5	Oil shale	78.10	146.00	16.70	75.50	14.90	3.68	17.00	3.25	17.30	3.48	8.69	1.37	7.10	0.99	394.06	5.66	0.75	0.96
TY2-6	Oil shale	75.50	165.00	17.90	74.40	13.10	2.82	12.10	1.94	10.50	2.18	6.27	1.11	6.48	0.90	390.20	8.41	0.73	1.07
TY2-7	Mudstone	64.60	99.40	13.20	52.40	9.69	1.97	7.82	1.41	6.98	1.45	4.22	0.67	4.29	0.60	268.70	8.79	0.74	0.81
TY2-8	Mudstone	69.60	134.00	15.90	62.40	11.60	2.30	9.77	1.81	9.66	2.00	5.80	0.93	5.86	0.85	332.48	8.06	0.70	0.96
TY2-10	Mudstone	64.90	144.00	14.70	63.70	10.70	2.44	10.80	1.81	9.80	2.01	5.11	0.89	4.99	0.75	336.60	8.31	0.74	1.11
TY2-11	Oil shale	67.96	128.96	14.67	60.16	10.94	2.54	10.83	1.97	10.19	2.03	5.54	0.90	5.20	0.73	322.62	7.63	0.76	0.97
TY2-12	Mudstone	87.70	173.00	19.70	75.00	13.50	2.82	12.00	2.10	10.40	2.09	5.79	0.93	5.85	0.81	411.69	9.30	0.72	0.99
TY2-14	Oil shale	74.60	118.00	13.90	54.70	9.75	2.35	9.59	1.86	9.05	1.68	4.66	0.72	4.41	0.60	305.87	8.39	0.79	0.87
TY2-15	Mudstone	123.00	226.00	23.90	89.20	16.40	3.82	13.60	2.64	11.80	2.16	5.80	0.94	5.26	0.68	525.21	11.25	0.83	0.99
TY2-16	Mudstone	252.00	545.00	51.10	191.00	32.40	7.57	30.40	5.58	24.70	4.13	10.30	1.34	7.32	0.91	1163.75	12.74	0.79	1.14
TY2-20	Mudstone	191.00	345.00	30.80	109.00	16.70	3.56	15.40	2.78	12.90	2.54	6.80	1.14	6.60	0.84	745.06	14.21	0.72	1.07
TY2-21	Oil shale	34.60	53.80	6.57	23.60	4.83	0.99	4.27	0.94	4.89	0.99	2.97	0.47	2.86	0.41	142.19	6.99	0.71	0.85
TY2-22	Mudstone	57.10	122.00	12.60	47.70	8.32	1.59	7.36	1.25	6.59	1.29	3.86	0.67	4.01	0.59	274.93	9.73	0.66	1.08
Chondrite*		0.31	0.81	0.12	0.60	0.20	0.07	0.26	0.05	0.32	0.07	0.21	0.03	0.21	0.03	3.29			

* Chondrite data from [35]. Abbreviations: REE – rare earth elements, LREE – light rare earth elements, HREE – heavy rare earth elements, δEu – europium anomaly, δCe – cerium anomaly.

5. Discussion

5.1. Paleoclimate

The C-value, Sr/Cu, and Rb/Sr ratios are common indicators of paleoclimate [37, 38]. The formula for the C-value is as follows [12]:

$$C = w(V + Ni + Mn + Fe + Cr + Co) / w(Ca + Mg + Ba + Sr + Na + K). \quad (1)$$

The C-value of 0.2 indicates an arid paleoclimate, 0.2–0.6 shows a semi-humid to semi-arid paleoclimate, and >0.6 denotes a humid paleoclimate [39]. The Sr/Cu ratio <10 indicates a warm and humid paleoclimate, and >10 shows an arid paleoclimate [39]. High Rb/Sr ratios imply warm and humid climate [40].

It should be noted that an increase in carbonate can cause the enrichment of Sr, which in turn leads to an increase in the Sr/Cu ratio and a decrease in the Rb/Sr ratio. However, these changes are not related to the paleoclimate. The plot of Sr vs. CaO shows no significant relationship between them, indicating that Sr content is not affected by carbonate (Fig. 5). In this case, Sr/Cu and Rb/Sr ratios can be used as indicators of paleoclimate.

In this study, the C-values of the samples range from 0.23 to 0.96, with an average of 0.56. The Sr/Cu ratios range from 1.58 to 20.68, with an average of 5.94, and the Rb/Sr ratios range from 0.09 to 1.71, with an average of 0.62. Even excluding samples with Rb/Sr ratios greater than 1, the average still reaches 0.46 (Table 4). These indicators suggest that the paleoclimate was warm and humid.

Furthermore, paleoclimate is mainly influenced by the paleolatitude of the study area. Previous studies show that the paleolatitude of the Qaidam Basin was lower than it is today [41, 42], and according to Halim et al. [42], the Late

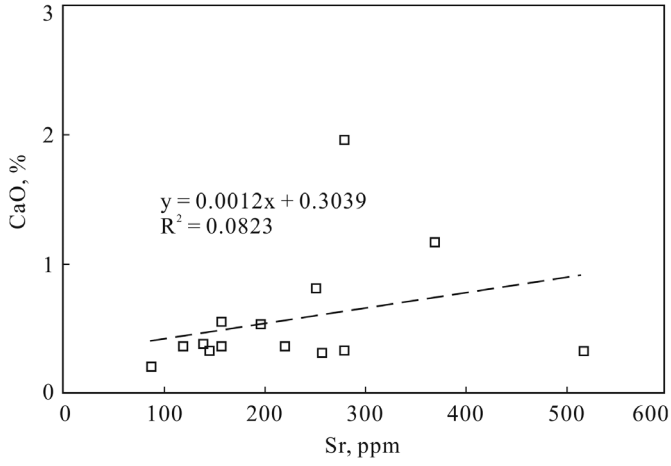

Fig. 5. Plot of Sr vs. CaO.

Jurassic paleolatitude of the Huatugou region, located north of the Qaidam Basin, was 19.2° N. Additionally, paleopalynological studies from the J_2sh^1 of the Qaidam Basin show a combination of *Alsophila* and *Lycopodiumsporites*, which indicate a warm and humid climate [43]. Therefore, both paleolatitude and paleopalynology support the conclusion of a warm and humid paleoclimate in J_2sh^1.

Table 4. Geochemical parameters of J_2sh^1 in the Tuanyushan area, Qaidam Basin

Sample	Lithology	C-value	Rb/Sr	Sr/Cu	Sr/Ba	Th/U	100Mg/Al	(Cu + Mo)/Zn	δU	Mo_{EF}	U_{EF}
TY2-2	Mudstone	0.34	0.48	4.26	0.03	3.04	4.02	1.16	0.99	1.16	2.08
TY2-3	Oil shale	0.52	1.08	3.09	0.14	2.98	3.81	0.89	1.00	3.33	3.02
TY2-4	Mudstone	0.23	0.73	5.24	0.24	4.49	96.21	0.47	0.80	0.44	1.97
TY2-5	Oil shale	0.52	0.26	3.51	0.26	2.57	3.40	0.76	1.08	3.41	3.31
TY2-6	Oil shale	0.58	0.29	2.87	0.12	2.26	4.09	1.42	1.14	6.32	4.35
TY2-7	Mudstone	0.41	0.68	11.08	0.37	4.52	3.58	0.35	0.80	0.51	1.41
TY2-8	Mudstone	0.86	0.97	1.58	0.33	5.52	3.94	0.77	0.70	0.88	1.41
TY2-10	Mudstone	0.96	1.23	3.42	0.28	4.43	4.44	0.35	0.81	2.44	1.54
TY2-11	Oil shale	0.38	0.34	3.64	0.18	3.07	4.70	0.34	0.99	7.00	4.14
TY2-12	Mudstone	0.79	0.94	3.24	0.15	5.55	3.95	0.42	0.70	1.13	1.34
TY2-14	Oil shale	0.55	0.31	12.15	0.58	3.82	0.81	0.03	0.88	2.91	1.51
TY2-15	Mudstone	0.51	0.24	11.92	0.22	4.40	0.96	0.26	0.81	2.60	2.03
TY2-16	Mudstone	0.56	0.48	1.88	0.22	2.00	0.99	0.77	1.20	3.33	5.16
TY2-20	Mudstone	0.48	0.11	20.68	0.68	3.67	0.79	0.56	0.90	3.44	1.68
TY2-21	Oil shale	0.89	0.09	3.18	0.12	4.60	1.90	1.99	0.79	9.86	2.13
TY2-22	Mudstone	0.34	1.71	3.37	0.17	3.10	3.66	0.29	0.98	0.82	2.22

5.2. Paleosalinity

Sr/Ba, Th/U, and values of 100 × Mg/Al are common indicators of paleosalinity [44–46]. Sr/Ba ratios of <0.6, 0.6–1, and >1 reflect saline, brackish, and freshwater conditions, respectively [46]. Th/U ratios of <2, 2–7, and >7 indicate saline, brackish, and freshwater conditions, respectively [44]. Furthermore, values of 100 × Mg/Al >10, 1–10, and <1 represent saline, brackish, and freshwater conditions, respectively [45].

In this study, the Sr/Ba ratios of the samples range from 0.03 to 0.68, with an average of 0.26; the Th/U ratios vary from 2.00 to 5.52, with an average of

3.75; and the values of 100 × Mg/Al of most samples range from 0.79 to 4.44, with an average of 3.0, except one anomalously high value (Table 4). These indicators show that the paleosalinity conditions were mainly freshwater to brackish.

5.3. Redox conditions

δU and (Cu + Mo)/Zn ratios are commonly used to indicate redox conditions [47, 48]. The formula for δU is as follows:

$$\delta U = 2U / (U + Th/3), \quad (2)$$

where δU values <1 indicate reducing environments [47]. Meanwhile, the (Cu + Mo)/Zn ratio increases as oxygen availability decreases [48], and some scholars believe that ratios <0.55 represent oxic conditions [49]. In this study, the δU ratios range from 0.70 to 1.24, with an average of 0.91, and (Cu + Mo)/Zn ratios vary from 0.03 to 1.99, with an average of 0.68, indicating that the redox conditions in the studied area are generally anoxic (Table 4).

Additionally, the plot of Mo_{EF} vs. U_{EF} can also be used to indicate redox conditions [50], where the elemental enrichment factor (EF) is calculated as follows:

$$X_{EF} = (X/Al)_{sample} / (X/Al)_{PAAS}, \quad (3)$$

where X and Al represent the weight percentages of the elements X and Al, respectively, and the subscripts $_{sample}$ and $_{PAAS}$ represent the values of the samples and those of PAAS [50]. The plot of Mo_{EF} vs. U_{EF} further supports the conclusion that the redox conditions in the study area are generally anoxic (Fig. 6).

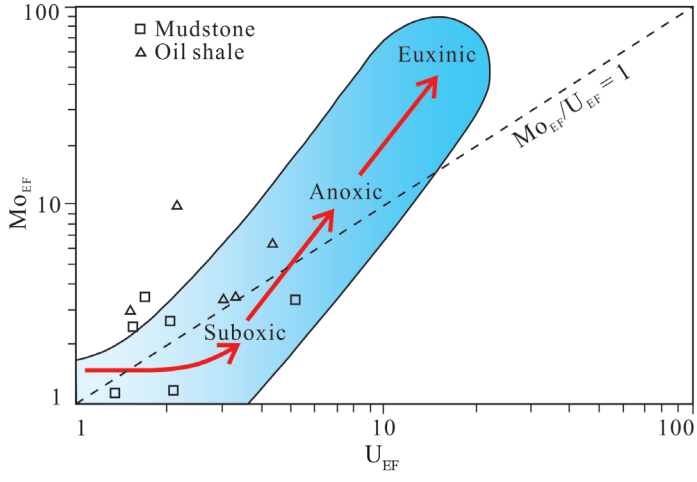

Fig. 6. Plot of Mo_{EF} vs. U_{EF} ratios.

5.4. Paleoweathering

The chemical index of alteration (CIA) can be used to represent the weathering intensity and paleoclimate conditions of the source area [33]. The CIA is calculated as follows:

$$CIA = [Al_2O_3 / (Al_2O_3 + CaO^* + Na_2O + K_2O)] \times 100, \quad (4)$$

where the major element concentrations are expressed in mol%, and CaO* refers to the CaO content in silicate minerals, excluding its presence in carbonates or apatite. According to the McLennan method [51], CaO content can be corrected based on the P_2O_5 content, and the corrected CaO and Na_2O contents can then be compared, with CaO* equaling the lower value.

High CIA values indicate significant loss of Ca, Na, and K relative to Al, reflecting a relatively strong weathering degree typical of a warm and humid climate. Based on this principle, Fedo et al. [52] categorize weathering intensity and paleoclimate conditions into three grades: CIA values between 50 and 60 indicate a low degree of chemical weathering, corresponding to a cold and arid climate; CIA values between 60 and 80 show a moderate degree of chemical weathering, typical of a warm and humid climate; and CIA values between 80 and 100 reflect a high degree of weathering, indicative of a hot and humid climate.

However, it is necessary to consider the effects of potassium metasomatism and sedimentary recycling when using CIA values to indicate paleoweathering conditions [52]. Kaolinite is transformed into illite by potassium metasomatism, reducing the calculated CIA value below the true CIA value [33]. Conversely, sedimentary recycling enriches sediments with clay minerals, such as kaolinite,

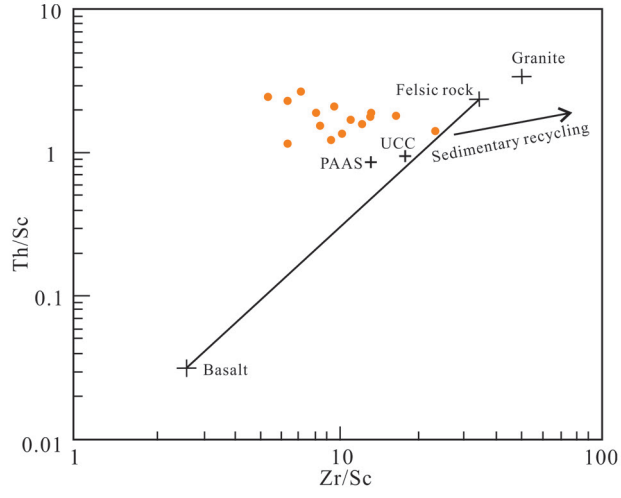

Fig. 7. Plot of Zr/Sc vs. Th/Sc [51] for J_2sh^1 in the QCD-2 well, Tuanyushan area, Qaidam Basin.

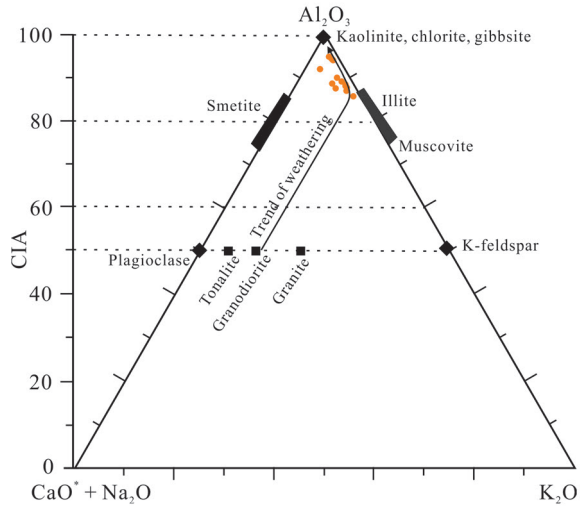

Fig. 8. Al_2O_3 – (CaO* + Na_2O) – K_2O ternary diagram for J_2sh^1 samples [52].

montmorillonite, and sericite, increasing the calculated CIA value above the true CIA value [52].

In this study, a plot of Zr/Sc vs. Th/Sc is used to determine whether these samples have experienced sedimentary recycling, and the Al_2O_3 – (CaO* + Na_2O) – K_2O ternary diagram is applied to analyze potassium metasomatism and correct the CIA values. Figure 7 shows that the samples did not undergo sedimentary recycling; thus, it has no influence on the CIA. Figure 8 demonstrates that the samples follow a desirable weathering trend (solid arrow line in Fig. 8), confirming that the CIA values indicate the true weathering conditions. The CIA values range from 86.4 to 95.6, indicating strong weathering conditions.

5.5. Provenance

Sedimentary recycling often leads to the enrichment of heavy minerals, causing the enrichment of some elements [53]. This enrichment can influence the results of proposed provenance. Therefore, it is necessary to analyze sedimentary recycling before conducting provenance analyses. The plot of Zr/Sc vs. Th/Sc is used to evaluate sedimentary recycling. Figure 7 shows that the samples do not undergo sedimentary recycling, validating the use of geochemical data for provenance analysis.

Al_2O_3/TiO_2 ratios, TiO_2/Zr ratios, and the plots of Al_2O_3 vs. TiO_2 and TiO_2 vs. Zr are used to determine the provenance [12]. In this study, Al_2O_3/TiO_2 ratios range from 22.99 to 37.02, with an average of 30.14, and TiO_2/Zr ratios vary from 23.04 to 76.47, with an average of 48.36, indicating that the main provenance is felsic igneous rocks. The plots of Al_2O_3 vs. TiO_2 and TiO_2 vs. Zr

also show that the main provenance is felsic igneous rocks, and the secondary provenance is intermediate igneous rocks (Fig. 9).

Trace elements and REEs have varying enrichment degrees in different types of source rocks. For example, Sc, Ni, Cr, and Co tend to be enriched in basic rocks, while La, Th, Hf, Zr, and REEs are enriched in acid rocks [54]. Based on this feature, previous researchers have developed discrimination diagrams of trace elements and REEs to indicate provenance. In this study, plots of La/Th vs. Hf, Co/Th vs. La/Sc, and La/Yb vs. ΣREE [34, 55–57] are used for provenance analysis. The plot pf La/Th vs. Hf shows that the provenance is mainly acidic arc source with contributions from a mixed felsic/basic source, while one sample shows an old sedimentary component (Fig. 10a). The plot of Co/Th vs. La/Sc reveals that the provenance of most samples is felsic igneous rocks, with two samples suggesting an intermediate igneous origin, possibly andesitic (Fig. 10b). The plot of La/Yb vs. ΣREE suggests that the provenance is granite, alkali basalt, and calcareous mudstone (Fig. 10c).

To sum up, the provenance is mainly felsic igneous rocks, with small amounts of intermediate rocks and sedimentary or basic rocks.

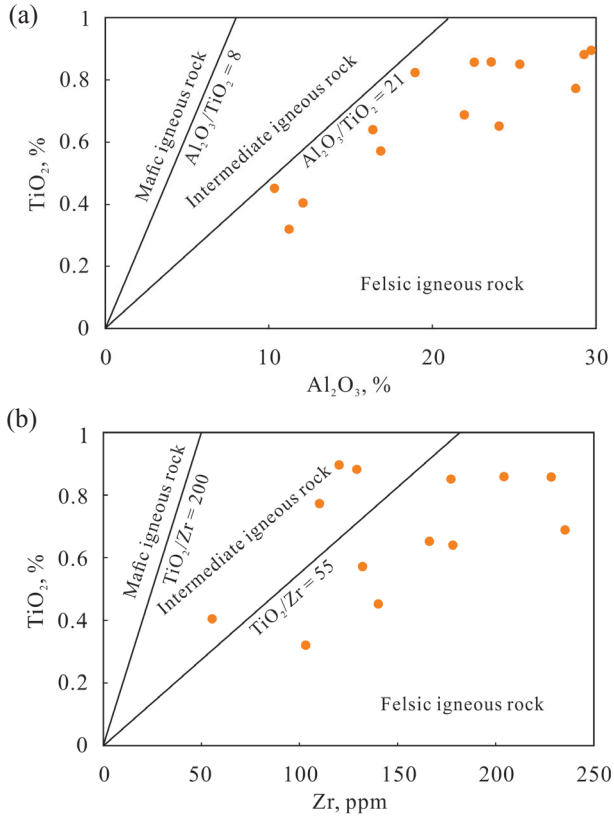

Fig. 9. Plots of (a) TiO_2 vs. Al_2O_3 [12] and (b) TiO_2 vs. Zr [12] for the mudstones of J_2sh^1 in the QCD-2 well.

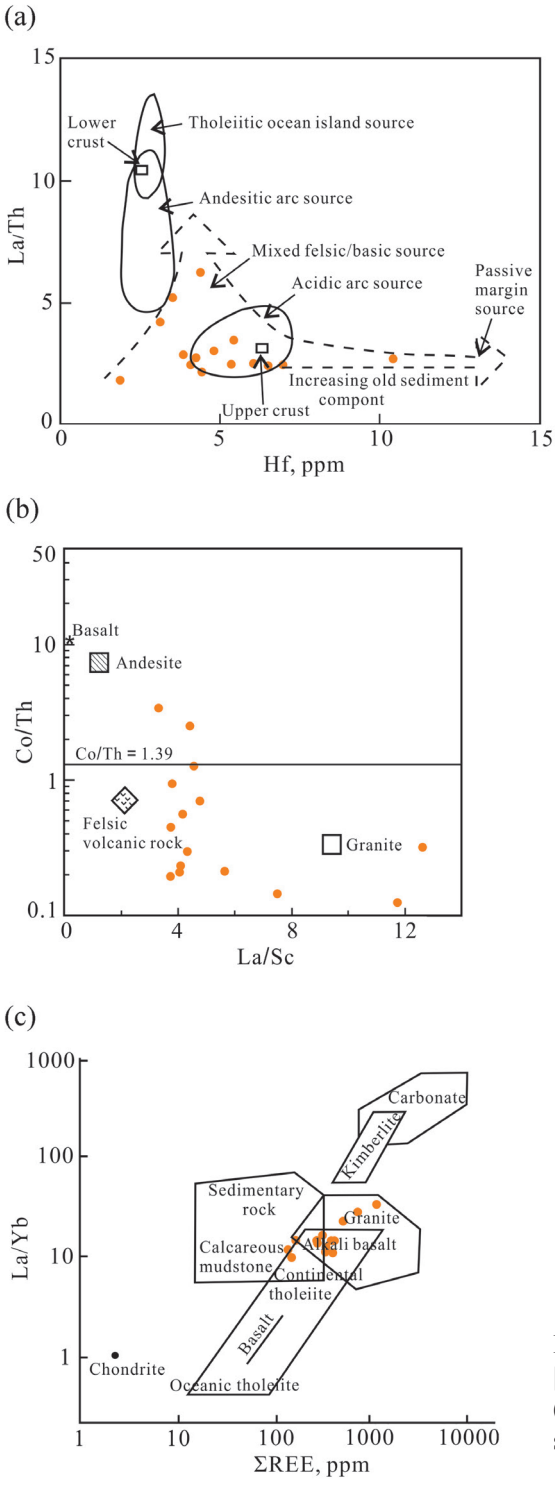

Fig. 10. Plots of (a) La/Th vs. Hf [34], (b) Co/Th vs. La/Sc [56] and (c) La/Yb vs. ΣREE [57] for the samples of J_2sh^1 in the QCD-2 well.

5.6. Tectonic setting of the source area

Bhatia and Crook [58] classified tectonic settings into four types based on the trace and REE compositions of Paleozoic graywacke in Australia: oceanic island arc (OIA), continental island arc (CIA), active continental margin (ACM), and passive margin (PM).

The four tectonic settings can be distinguished by major and trace elements and their ratios. The TiO_2 contents of the samples from the study area range from 0.32% to 1.04%, with an average value of 0.69; the (TFe_2O_3 + MgO) contents vary from 1.11% to 4.68%, with an average value of 2.35% (excluding the anomalous value of sample TY2-4); the SiO_2/Al_2O_3 ratios range from 1.45 to 3.35, with an average value of 1.96; and the K_2O/Na_2O ratios vary from 1.01 to 18.76, with an average value of 9.32. These values are the closest to the values of PM [58].

Diagrams of major elements or major element ratios can be used to indicate the tectonic setting, such as plots of TiO_2 vs. (TFe_2O_3 + MgO) and SiO_2/Al_2O_3 vs. K_2O/Na_2O [59]. In the TiO_2 vs. (TFe_2O_3 + MgO) plot, most samples fall outside the four tectonic setting fields, with only two samples located in the PM field (Fig. 11a). In the SiO_2/Al_2O_3 vs. K_2O/Na_2O plot, most samples are in the PM and ACM fields (Fig. 11b). Based on major elements, Bhatia [60] developed a discriminant function diagram (Fig. 11c). According to this diagram, most samples are in the PM field, except for one sample in the OIA field. Armstrong-Altrin [61] also proposed a discriminant function-based major element diagram for the tectonic discrimination of low siliciclastic sediments, where low silica corresponds to $(SiO_2)_{adj}$ = 35–63% (Fig. 11d). $(SiO_2)_{adj}$ refers to the SiO_2 value obtained after volatile-free adjustment of the ten major elements to 100 wt%. As shown in Figure 11d, most samples are in the rift and collision fields. The ACM field comprises sediments from arc and collision settings, and the PM field includes sediments from rift settings [13]. Therefore, Figure 11d indicates the tectonic settings of PM and ACM.

Trace elements and REEs, such as La, Th, Sc, Zr, Y, and Cr, can also be used to distinguish tectonic settings, since they are relatively stable during weathering and migration [62]. In the Sc/Cr vs. La/Y diagram, most of the samples fall outside the four tectonic setting fields, and only a part of samples are in the PM and ACM fields (Fig. 12a). In the La-Th-Sc ternary diagram, most samples are in the PM and ACM fields (Fig. 12b).

These diagrams and ratios indicate that the tectonic setting of the study area is either PM or ACM, with most pointing to PM. Bhatia [60] reported that ACM is typically characterized by fractionated REE patterns with a wide range of negative Eu anomalies, while PM presents uniform REE patterns with distinct negative Eu anomalies. In this study, δEu shows distinct negative anomalies (ranging from 0.58 to 0.83, with an average value of 0.73), and δCe shows slight negative anomalies (average of 0.99), indicating that the predominant tectonic setting is PM [36].

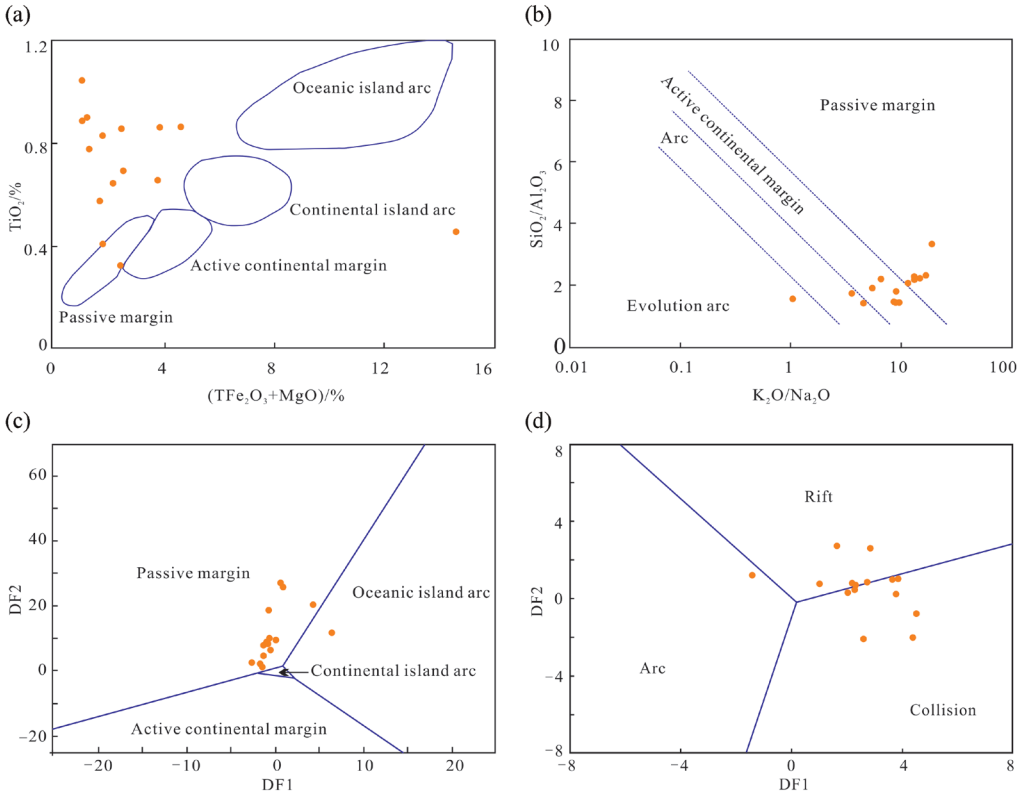

Fig. 11. (a) Plot of TiO_2 vs. (TFe_2O_3 + MgO) [60], (b) plot of SiO_2/Al_2O_3 vs. K_2O/Na_2O [59], (c) discriminant function (DF) diagram for four tectonic settings [60], (d) multidimensional DF diagram [61] for low-silica clastic sediments from three tectonic settings (arc, continental rift, and collision) for J_2sh^1 in the QCD-2 well. DF1 = (0.0447 × SiO_2) + (–0.972 × TiO_2) + (0.008 × Al_2O_3) + (0.267 × Fe_2O_3) + (0.208 × FeO) + (3.082 × MnO) + (0.140 × MgO) + (0.195 × CaO) + (0.719 × Na_2O) + (0.032 × K_2O) + (7.510 × P_2O_5) + 0.303; DF2 = (0.421 × SiO_2) + (1.988 × TiO_2) + (–0.526 × Al_2O_3) + (0.551 × Fe_2O_3) + (1.610 × FeO) + (2.720 × MnO) + (0.881 × MgO) + (0.907 × CaO) + (0.177 × Na_2O) + (1.840 × K_2O) + (7.244 × P_2O_5) + 43.57. DF1 (arc, rift, collision) = (0.608 × $\ln(Ti_2O/SiO_2)_{adj}$) + (–1.854 × $\ln(Al_2O_3/SiO_2)_{adj}$) + (0.299 × $\ln(TFe_2O_3/SiO_2)_{adj}$) + (–0.550 × $\ln(MnO/SiO_2)_{adj}$) + (0.120 × $\ln(MgO/SiO_2)_{adj}$) + (0.194 × $\ln(CaO/SiO_2)_{adj}$) + (–1.510 × $\ln(Na_2O/SiO_2)_{adj}$) + (1.941 × $\ln(K_2O/SiO_2)_{adj}$) + (0.003 × $\ln(P_2O_5/SiO_2)_{adj}$); DF2 (arc, rift, collision) = (–0.554 × $\ln(Ti_2O/SiO_2)_{adj}$) + (–0.995 × $\ln(Al_2O_3/SiO_2)_{adj}$) + (1.765 × $\ln(TFe_2O_3/SiO_2)_{adj}$) + (–1.391 × $\ln(MnO/SiO_2)_{adj}$) + (–1.034 × $\ln(MgO/SiO_2)_{adj}$) + (0.225 × $\ln(CaO/SiO_2)_{adj}$) + (0.713 × $\ln(Na_2O/SiO_2)_{adj}$) + (0.330 × $\ln(K_2O/SiO_2)_{adj}$) + (0.637 × $\ln(P_2O_5/SiO_2)_{adj}$).

5.7. Implications for the formation of oil shale

He et al. [63] inferred that the main erosion source area for the northern Qaidam Basin during the Jurassic was the Qilian orogenic belt, based on the characteristics of heavy mineral assemblages combined with the paleocurrent direction. Wang et al. [64] suggested that the source tectonic setting was a re-cyclical orogenic belt, with the Qilian Mountains in the north identified as the source area, based on an analysis of the source tectonic setting of the Shimengou Fm sandstone in the Yuqia area, which has the same tectonic setting and is located east of the Tuanyushan. Li et al. [1] revealed that during the Middle Jurassic, the main source area for the Tuanyushan was the Saishiteng Mountain in the northern Qilian Mountains, based on lithofacies and paleogeography. Feng et al. [65] found that the main sources of the eastern section were the Zongwulong Mountain, the Qaidam Mountain, and the Maoniu Mountain within the Qilian Mountains. Overall, previous studies considered the Qilian orogenic belt as the main provenance of the northern Qaidam Basin [66].

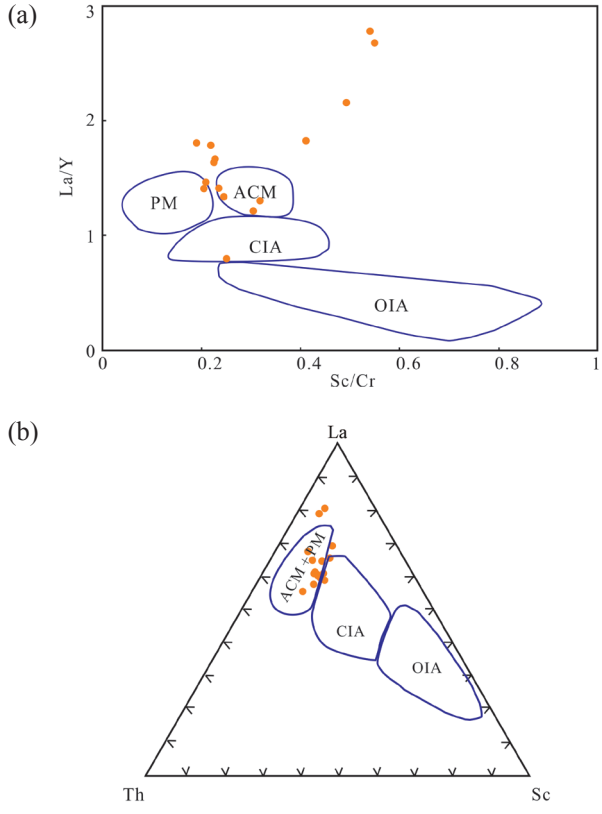

Fig. 12. Trace element tectonic discrimination diagrams: (a) Sc/Cr vs. La/Y [58]; (b) La-Th-Sc [58] for the samples of J_2sh^1 in the QCD-2 well. Abbreviations: PM – passive margin, ACM – active continental margin, CIA – continental island arc, OIA – oceanic island arc.

The Tuanyushan study area is located in the central part of the northern Qaidam Basin, geographically positioned in the southern part of the Saishiteng Mountain belonging to the Qilian Mountains (Figs 1, 13). The main source area for this region during the Middle Jurassic was the Saishiteng Mountain. As analyzed in Sections 5.4 and 5.5 of this study, the provenance is mainly felsic igneous rocks, with small amounts of intermediate, sedimentary, or basic rocks. The dominant tectonic setting is PM, with some characteristics of ACM. Therefore, the provenance can be attributed to different source rocks of the Saishiteng Mountain.

The Saishiteng Mountain and its surrounding areas mainly consist of Precambrian basement rocks, and Paleozoic igneous, sedimentary, and metamorphic rocks [67], including the Early Proterozoic Dakendaban Group crystalline metamorphic rocks, which constitute the Precambrian basement, intrusive rocks from the Caledonian and Hercynian periods, volcanic rocks, pyroclastic rocks, and metamorphic rocks of the Ordovician Tanjianshan Group, as well as sedimentary rocks interbedded with andesite and andesite basalt of the Upper Devonian [68]. The tectonic setting of the northern Qaidam Basin during the Early Proterozoic Dakendaban Group was PM [69], which transitioned to ACM in the Caledonian period [70] and remained ACM in the Ordovician [71]. From the Devonian to Early Permian, the tectonic setting of the northern Qaidam Basin was PM [72]. During the Middle Jurassic, the main provenance of the Tuanyushan area was Permian to Late Triassic rocks [67].

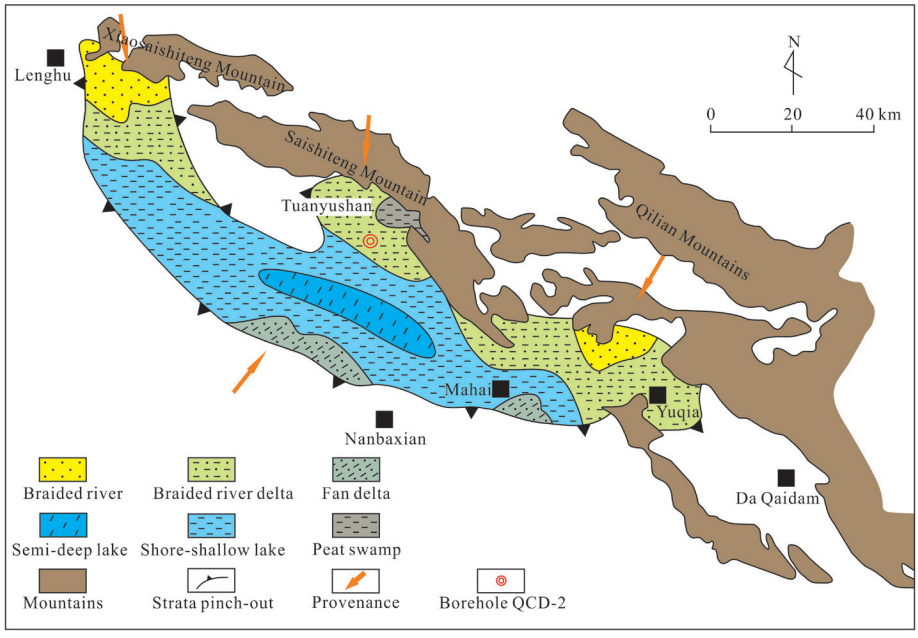

Fig. 13. Paleogeographic map of the Middle Jurassic in the Tuanyushan area of the Qaidam Basin [64].

Previous analysis shows that the primary tectonic setting of the source rocks in the study area was PM, and the main source rocks of J_2sh^1 are felsic rocks, suggesting that the main provenance came from Hercynian magmatic rocks of the Saishiteng Mountain in the Qilian Mountains, while other possible sources include the Early Proterozoic Dakendaban Group, Caledonian intrusive rocks, Ordovician Tanjianshan Group, and Upper Devonian rocks.

During the Early Jurassic, an extensional tectonic environment formed between the North China Block and the Qaidam Block, caused by differences in the northward migration rates of the North China Block, the Qaidam Block, the Tarim Block, and the Yangzi Block [73]. During this period, faulted basins developed in the northern Qaidam Basin [74]. During the Middle Jurassic, the extensional tectonic environment in the northern Qaidam Basin persisted, and migration rate differences continued to exist. The eastward migration of the Tarim Block and the northward drift of the Qiangtang Block resulted in a simultaneous compression of the western and southern sections of the Qaidam Block (Fig. 14). Combined with the rotation of the Qaidam Block, the western part of the northern Qaidam Basin transformed from an extensional to a compressive tectonic environment. Under the influence of these tectonic processes, the northern Qaidam Basin experienced strong fault subsidence in the eastern part and relatively small tectonic subsidence in the western part. The Tuanyushan study area, located in the midwest of the northern Qaidam Basin, showed small subsidence and a relatively stable tectonic environment in J_2sh^1.

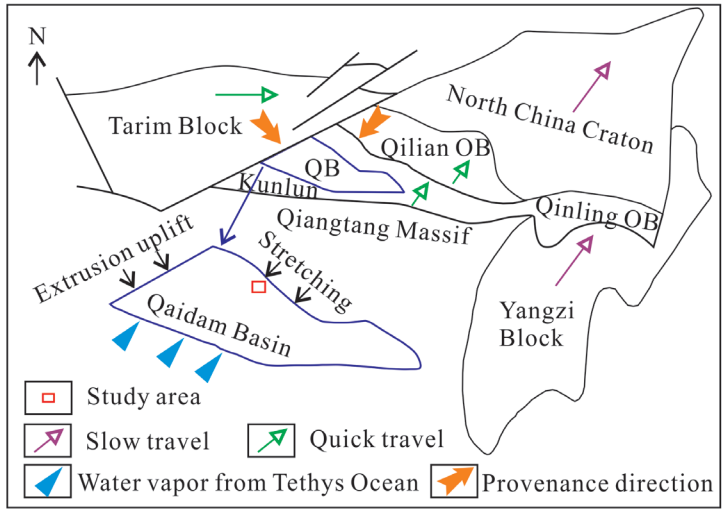

Fig. 14. Model showing the tectonic, climatic, and depositional systems during the Middle Jurassic in the Qaidam Basin [73]. Abbreviations: QB – Qaidam Basin, OB – orogenic belt.

During the Middle Jurassic, the sedimentary environment of the Lenghu–Tuanyushan–Yuka area was mainly a faulted lake basin. Sedimentary facies, such as semi-deep lake, shore-shallow lake, peat swamp, and braided driver delta, were developed in this region. The QCD-2 well and its surrounding sedimentary environment primarily comprised peat swamps, braided river deltas, and shallow lakes (Fig. 13). According to the Walther's law of facies, these sedimentary facies are also present in the QCD-2 well (Fig. 2). The sedimentary facies in the QCD-2 well changed with variations in the depth of the lake basin. When the water was shallow, a peat swamp environment developed, leading to coal formation. When the water was deeper, a shallow lake environment emerged, resulting in the formation of oil shale [8].

During the Middle Jurassic, the tectonic environment of the Tuanyushan was relatively stable. The climate of the study area was warm and humid due to its low paleolatitude [42] and water vapor from the Tethys Ocean in the southwest of the Qaidam Basin [73] (Fig. 14). This climate provided favorable conditions for the proliferation of organisms. The source rocks of the Saishiteng Mountain in the northern part of the basin were strongly weathered and then transported by wind and water into the lake basin.

In the J_2sh^1, during water regression periods, the water depth of the study area was relatively low, fostering the development of a peat swamp environment. The main organic matter at this time primarily originated from higher plants imported from land. Plant fragments accumulated, compacted, and were gradually transformed into peat by microorganisms. After further burial and metamorphism, peat formed coal.

During flooding periods, the sedimentary environment changed to a shallow lake due to the increase in water depth. Deeper water supported the proliferation of aquatic organisms, such as algae. At the same time, the paleosalinity was freshwater to brackish, and the nutrients carried by terrigenous debris promoted the reproduction of lake organisms. However, due to the short flooding time and shallow water depth, the total amount of lake organisms was not very abundant. These aquatic organisms, together with the continuous input of abundant terrestrial plant debris, provided a rich material basis for the formation of organic matter. The redox conditions were generally anoxic, enabling the preservation of organic matter, which resulted in the formation of oil shale (Fig. 15).

Multiple and short-term floods resulted in the co-development of coal and oil shale (Fig. 2). Since the organic matter in the oil shale is rich in terrestrial inputs, the proportion of organic matter converted into oil is relatively low. Consequently, the oil shale has a high TOC content (TOC_{max} 34.10%) and a relatively moderate oil yield (oil $yield_{max}$ 7.74%; Figs 2, 15).

Furthermore, the tectonic setting of the source area, paleoclimate, and sedimentary environment of J_2sh^1 contribute to the understanding of the tectonic and paleogeographic evolution of the Eastern Tethys, particularly the tectonic and sedimentary context of the Middle Jurassic.

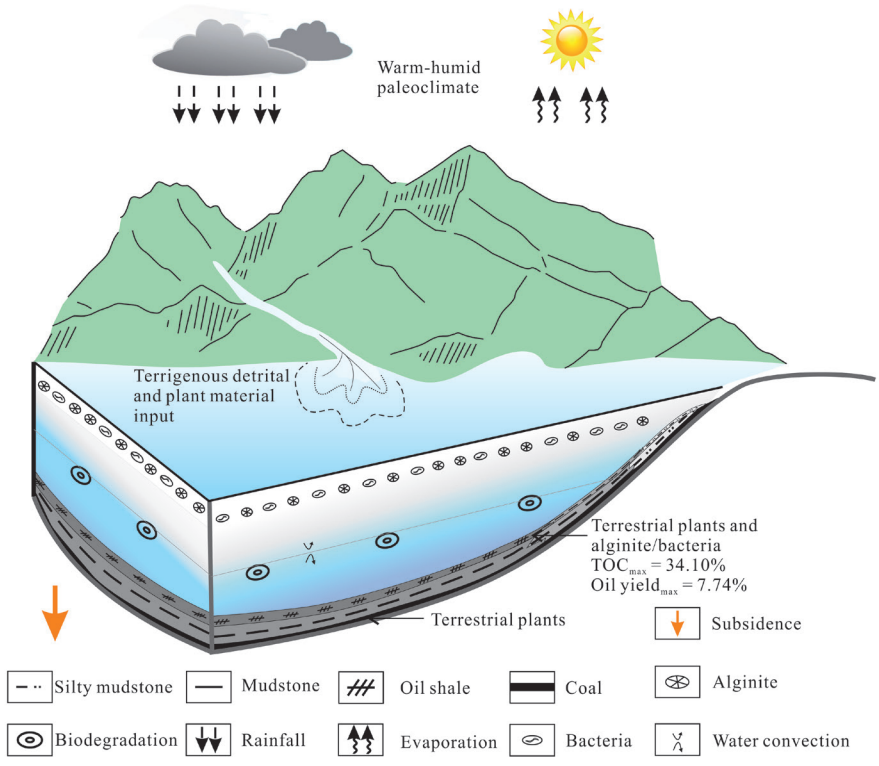

Fig. 15. Formation model of J_2sh^1 oil shale in the Tuanyushan area of the Qaidam Basin.

6. Conclusions

1. The provenance of the J_2sh^1 oil shale and mudstone in the Tuanyushan area of the northern Qaidam Basin is mainly felsic rocks. Its source area is the Saishiteng Mountain in the Qilian Mountains, and the provenance primarily consists of Hercynian intrusive rocks. During the Middle Jurassic period, these source rocks entered the northern Qaidam Basin after intense weathering.
2. During the Middle Jurassic, the tectonic setting of the Tuanyushan area was stable, the paleoclimate was warm and humid, the paleosalinity conditions ranged from freshwater to brackish, and the redox conditions were generally anoxic. These factors provided favorable conditions for the formation of oil shale and coal.
3. During the Middle Jurassic, the favorable mineralization background of the Tuanyushan area provided a favorable environment for the

development of terrestrial plants and aquatic organisms. During water regression periods, abundant terrestrial plants formed coal, while during flooding periods, the increasing water depth and the input of nutrients from terrestrial debris promoted the development of lake algae. Algae and other lake organisms, as well as terrestrial plants, provided the material basis for the formation of organic matter. The anoxic preservation conditions enabled the preservation of organic matter, resulting in the formation of oil shale.

Data availability statement

Data are contained within the article.

Acknowledgments

This study was financially supported by the National Natural Science Foundation of China (grants No. 52374010 and No. 41472173), the Ministry of Land and Resources Outstanding Youth Science and Technology Talent Training Program of China (grant No. 201311111), the Program of China Geological Survey (grants No. DD20242509 and No. DD20242050), and the Program of Oil and gas Survey, China Geological Survey (grant No. YKC-2023-YC01). The authors sincerely thank all reviewers for their abundant critical and constructive comments. The publication costs of this article were partially covered by the Estonian Academy of Sciences.

References

1. Li, M., Shao, L. Y., Lu, J., Baruch, S., Wen, H. J., Li, Y. H. Sequence stratigraphy and paleogeography of the Middle Jurassic coal measures in the Yuqia coalfield, northern Qaidam Basin, northwestern China. *AAPG Bull.*, 2014, **98**(12), 2531–2550. https://doi.org/10.1306/06041413129
2. Guo, T. X., Ren, S. M., Luo, X. R., Bao, S. J., Wang, S. J., Zhou, Z., Chen, X. L., Li, H. H., Xu, Q. F. Accumulation conditions and prospective areas of shale gas in the Middle Jurassic Dameigou Formation, northern Qaidam Basin, Northwest China. *Geol. J.*, 2018, **53**(6), 2944–2954. https://doi.org/10.1002/gj.3134
3. Fu, S. T., Ma, D. D., Guo, Z. J., Cheng, F. Strike-slip superimposed Qaidam Basin and its control on oil and gas accumulation, NW China. *Petrol. Explor. Dev.*, 2015, **42**(6), 778–789. https://doi.org/10.1016/S1876-3804(15)30074-4
4. Tian, J., Li, J., Kong, H., Zeng, X., Wang, X., Guo, Z. Genesis and accumulation process of deep natural gas in the Altun foreland on the northern margin of the Qaidam Basin. *J. Petrol. Sci. Eng.*, 2021, **200**, 108147. https://doi.org/10.1016/j.petrol.2020.108147

5. Li, G. X., Zhu, R. K., Zhang, Y. S., Chen, Y., Cui, J. W., Jiang, Y. H., Wu, K. Y., Sheng, J., Xian, C. G., Liu, H. Geological characteristics, evaluation criteria and discovery significance of Paleogene Yingxiongling shale oil in Qaidam Basin, NW China. *Petrol. Explor. Dev.*, 2022, **49**(1), 21–36. https://doi.org/10.1016/S1876-3804(22)60002-8
6. Wang, J. X., Sun, P. C., Liu, Z. J., Xu, Y. B., Li, L. Evaluation of oil shale resources based on geochemistry and logging in Tuanyushan, Qaidam Basin, Northwest China. *Oil Shale*, 2020, **37**(3), 188–206. http://dx.doi.org/10.3176/oil.2020.3.02
7. Bai, Y. Y., Lv, Q. T., Liu, Z. J., Sun, P. C., Xu, Y. B., Meng, J. Y., Meng, Q. T., Xie, W. Q., Wang, J. X., Wang, K. B. Major, trace and rare earth element geochemistry of coal and oil shale in the Yuqia area, Middle Jurassic Shimengou Formation, northern Qaidam Basin. *Oil Shale*, 2020, **37**(1), 1–31. http://dx.doi.org/10.3176/oil.2020.1.01
8. Wang, J. X., Sun, P. C., Liu, Z. J., Li, L. Depositional environmental controls on the genesis and characteristics of oil shale: case study of the Middle Jurassic Shimengou Formation, northern Qaidam Basin, northwest China. *Geol. J.*, 2020, **55**(6), 4585–4603. https://doi.org/10.1002/gj.3688
9. Xu, Y. B., Sun, P. C., Yao, S. Q., Liu, Z. J., Tian, X. M., Li, F., Zhang, J. Q. Progress in exploration, development and utilization of oil shale in China. *Oil Shale*, 2019, **36**(2), 285–304. https://doi.org/10.3176/oil.2019.2.03
10. Rollinson, H. R. A terrane interpretation of the Archaean Limpopo Belt. *Geol. Mag.*, 1993, **130**(6), 755–765. https://doi.org/10.1017/S001675680002313X
11. Chen, L., Zhang, B., Jiang, S., Chen, X., Zhang, G., Zhang, J., Wei, W., Lu, Y., Chen, P., Lin, W. Provenance, source weathering, and tectonic setting of the lower Cambrian Shuijingtuo Formation in the middle Yangtze area, China. *Mar. Petrol. Geol.*, 2022, **139**, 105584. https://doi.org/10.1016/j.marpetgeo.2022.105584
12. Tao, S., Xu, Y. B., Tang, D. Z., Xu, H., Li, S., Chen, S. D., Liu, W. B., Cui, Y., Gou, M. F. Geochemistry of the Shitoumei oil shale in the Santanghu Basin, Northwest China: implications for paleoclimate conditions, weathering, provenance and tectonic setting. *Int. J. Coal. Geol.*, 2017, **184**, 42–56. https://doi.org/10.1016/j.coal.2017.11.007
13. Zhang, P. L., Meng, Q. T., Liu, Z. J., Hu, F. Mineralogy and geochemistry of the Lower Cretaceous Jiufotang Formation, Beipiao Basin, NE China: implications for weathering, provenance, and tectonic setting. *ACS Earth Space Chem.*, 2021, **5**(6), 1288–1305. https://doi.org/10.1021/acsearthspacechem.0c00216
14. Fu, L., Guan, P., Zhao, W. Y., Wang, M., Zhang, Y., Lu, J. W. Heavy mineral feature and provenance analysis of Paleogene Lulehe Formation in Qaidam Basin. *Acta Petrol. Sin.*, 2013, **29**(8), 2867–2875.
15. Jian, X., Guan, P., Zhang, D. W., Zhang, W., Feng, F., Liu, R. J., Lin, S. D. Provenance of Tertiary sandstone in the northern Qaidam basin, northeastern Tibetan Plateau: integration of framework petrography, heavy mineral analysis and mineral chemistry. *Sediment. Geol.*, 2013, **290**, 109–125. https://doi.org/10.1016/j.sedgeo.2013.03.010
16. Jian, X., Guan, P., Zhang, W., Feng, F. Geochemistry of Mesozoic and Cenozoic sediments in the northern Qaidam basin, northeastern Tibetan Plateau:

implications for provenance and weathering. *Chem. Geol.*, 2013, **360–361**, 74–88. https://doi.org/10.1016/j.chemgeo.2013.10.011

17. Zhu, W., Wu, C., Wang, J., Zhou, T., Li, J., Zhang, C., Li, L. Heavy mineral compositions and zircon U–Pb ages of Cenozoic sandstones in the SW Qaidam Basin, northern Tibetan Plateau: implications for provenance and tectonic setting. *J. Asian Earth Sci*., 2017, **146**, 233–250. https://doi.org/10.1016/j.jseaes.2017.05.023
18. Hong, D., Jian, X., Fu, L., Zhang, W. Garnet trace element geochemistry as a sediment provenance indicator: an example from the Qaidam Basin, northern Tibet. *Mar. Petrol. Geol.*, 2020. **116**, 104316. https://doi.org/10.1016/j.marpetgeo.2020.104316
19. Zhang, X., Gao, Z., Fan, T., Xue, J., Li, W., Zhang, H., Cao, F. Element geochemical characteristics, provenance attributes, and paleosedimentary environment of the Paleogene strata in the Lenghu area, northwestern Qaidam Basin. *J. Petrol. Sci. Eng.*, 2020, **195**, 107750. https://doi.org/10.1016/j.petrol.2020.107750
20. Li, C., Zheng, D., Zhou, R., Wang, W., Yu, J., Liu, C., Wang, Y., Pang, J., Ma, Y., Hao, Y., Li, Y., Wang, X. Topographic growth of the northeastern Tibetan Plateau during the Middle–Late Miocene: insights from integrated provenance analysis in the NE Qaidam Basin. *Basin Res*., 2021, **33**(6), 3212–3230. https://doi.org/10.1111/bre.12600
21. Shu, D., Xu, S., Wu, S., Li, S., Wang, D., Xiao, Y., Wu, X., Wang, J., Somerville, I. Jurassic sedimentary provenances of the Hongshan and Huobuxun sags in the eastern segment of the northern Qaidam Basin: basin–mountain coupling. *Geol. J.*, 2017, **52**(S1), 380–393.
22. Zhao, J., Zeng, X., Tian, J., Hu, C., Wang, D., Yan, Z., Wang, K., Zhao, X. Provenance and paleogeography of the Jurassic northwestern Qaidam Basin (NW China): evidence from sedimentary records and detrital zircon geochronology. *J. Asian Earth Sci.*, 2020, **190**, 104060.
23. Yuan, J., Liu, Y., Li, W., Jiang, L., Yuan, S., Li, S. Reconstruction of the early–middle Jurassic source-to-sink system in the western Qaidam Basin (North Tibet): constraints from zircon U–Pb ages of Jurassic sediments and granites. *J. Asian Earth Sci.*, 2020, **232**, 105164. https://doi.org/10.1016/j.jseaes.2022.105164
24. Zhang, X., Gao, Z., Fan, T., Xue, J., Li, W., Cao, F., Zhang, H. Geochemical characteristics, provenance and paleodepositional environment of the Lower Jurassic Huxishan Formation in the Lenghu area, northwestern Qaidam Basin, North West China: implications for organic matter origin. *J. Petrol. Sci. Eng*., 2021, **205**, 108951. https://doi.org/10.1016/j.petrol.2021.108951
25. Ritts, B. D., Hanson, A. D., Zinniker, D., Moldowan, J. M. Lower–Middle Jurassic nonmarine source rocks and petroleum systems of the northern Qaidam Basin, northwest China. *AAPG Bull.*, 1999, **83**(12), 1980–2005. https://doi.org/10.1306/E4FD4661-1732-11D7-8645000102C1865D
26. Wang, Y. X., Xu, S., Hao, F., Poulton, S. W., Zhang, Y. Y., Guo, T. X., Lu, Y. B., Bai, N. Arid climate disturbance and the development of salinized lacustrine oil shale in the Middle Jurassic Dameigou Formation, Qaidam Basin, northwestern

China. *Palaeogeogr., Palaeoclimatol., Palaeoecol.*, 2021, **577**, 110533. https://doi.org/10.1016/j.palaeo.2021.110533

27. Wu, Z., Grohmann, S., Littke, R., Guo, T., He, S., Baniasad, A. Organic petrologic and geochemical characterization of petroleum source rocks in the Middle Jurassic Dameigou Formation, Qaidam Basin, northwestern China: insights into paleo-depositional environment and organic matter accumulation. *Int. J. Coal Geol.*, 2022, **259**, 104038. https://doi.org/10.1016/j.coal.2022.104038
28. Yu, X., Guo, Z., Guan, S., Du, W., Wang, Z., Bian, Q., Li, L. Landscape and tectonic evolution of Bayin River watershed, northeastern Qaidam Basin, northern Tibetan Plateau: implications for the role of river morphology in source analysis and low temperature thermochronology. *J. Geophys. Res. Earth Surf.*, 2019, **124**(7), 1701–1719.
29. Tang, W. Q., Zhang, D. W, Zhou, Y. X., Liu, Y. Y., Wu, K. Y., Zhang, P. C., Han, Q. C., Li, F. J., Ma, C. Astronomical forcing in the coal-bearing Middle Jurassic Dameigou Formation, Qaidam Basin, northwestern China. *Ore Geol. Rev*., 2023, **161**, 105663. https://doi.org/10.1029/2018JF004989
30. Gong, S. L., Chen, N. S., Wang, Q. Y., Kusky, T. M., Wang, L., Zhang, L., Ba, J., Liao, F. Early Paleoproterozoic magmatism in the Quanji Massif, northeastern margin of the Qinghai–Tibet Plateau and its tectonic significance: LA-ICP-MS U–Pb zircon geochronology and geochemistry. *Gondwana Res.*, 2012, **21**(1), 152–166. https://doi.org/10.1016/j.gr.2011.07.011
31. Cao, J., Wu, M., Chen, Y., Hu, K., Bian, L., Wang, L., Zhang, Y. Trace and rare earth element geochemistry of Jurassic mudstones in the northern Qaidam Basin, northwest China. *Geochem.*, 2012, **72**(3), 245–252. https://doi.org/10.1016/j.chemer.2011.12.002
32. Ross, D. J. K., Bustin, R. M. Investigating the use of sedimentary geochemical proxies for paleoenvironment interpretation of thermally mature organic-rich strata: examples from the Devonian-Mississippian shales, Western Canadian Sedimentary Basin. *Chem. Geol.*, 2009, **260**(1–2), 1–19. https://doi.org/10.1016/j.chemgeo.2008.10.027
33. Nesbitt, H. W., Young, G. M. Early Proterozoic climates and plate motions inferred from major element chemistry of lutites. *Nature*, 1982, **299**, 715–717. http://dx.doi.org/10.1038/299715a0
34. Taylor, S. R., McLennan, S. M. *The Continental Crust: Its Composition and Evolution*. Blackwell Scientific Publications, Oxford, 1985.
35. Boynton, W. V. Geochemistry of the rare earth elements: meteorite studies. In: *Rare Earth Element Geochemistry* (Henderson, P., ed.). Elsevier, Amsterdam, 1984.
36. Haskin, L. A., Haskin, M. A., Frey, F. A., Wilderman, T. R. Relative and absolute terrestrial abundances of the rare earths. In: *Origin and Distribution of the Elements* (Ahrens, L. H., ed.). Pergamon, Oxford, 1968.
37. Jia, J. L., Liu, Z. J., Bechtel, A., Strobl, S. A., Sun, P. C. Tectonic and climate control of oil shale deposition in the Upper Cretaceous Qingshankou Formation (Songliao basin, NE China). *Int. J. Earth Sci*., 2013, **102**(6), 1717–1734. http://dx.doi.org/10.1007/s00531-013-0903-7

38. Ma, M., Lei, C., Rahman, M. J. J. Paleoenvironmental reconstruction of the Eocene sediments in the Baiyun sag of the Pearl River Mouth Basin. *Front. Earth Sci.*, 2023, **11**, 1177240. https://doi.org/10.3389/feart.2023.1177240
39. Yang, Y. Y., Liu, Y. Q., Zhou, D. W., Jiao, X., Cao, Q., Meng, Z. Y., Zhao, M. R. Lithotypes, organic matter and paleoenvironment characteristics in the Chang7_3 submember of the Triassic Yanchang Formation, Ordos Basin, China: implications for organic matter accumulation and favourable target lithotype. *J. Petrol. Sci. Eng.*, 2022, **216**, 110691. https://doi.org/10.1016/j.petrol.2022.110691
40. Xu, J. J., Jiang, J. C., Wang, D. Y., Xu, P., Wang, F. L., Li, H. Y., Cheng, X. G., Wu, Q. L., Cheng, F. Q., Lin, L. M., Xu, Y. B. Main controlling factors evolution on high-quality source rocks development in the Shanan Sag, Bohaibay Basin, NE China: implication from structure, depositional environment, and organic matter. *J. Asian Earth Sci.*, 2024, **263**, 106020. https://doi.org/10.1016/j.jseaes.2024.106020
41. Chen, Y., Gilder, S., Halim, N., Cogné, J. P., Courtillot, V. New paleomagnetic constraints on central Asian kinematics: displacement along the Altyn Tagh fault and rotation of the Qaidam Basin. *Tectonics*, 2002, **21**(5), 6-1–6-19. https://doi.org/10.1029/2001TC901030
42. Halim, N., Chen, Y., Cogné, J. P. A first palaeomagnetic study of Jurassic formations from the Qaidam basin, northeastern Tibet, China – tectonic implications. *Geophys. J. Int.*, 2003, **153**(1), 20–26. https://doi.org/10.1046/j.1365-246X.2003.01860.x
43. Yang, P., Xie, Z., Yuan, X., Zhu, S., Yi, D. Palaeoecological characteristics and its palaeogeographic significance of the Jurassic in northern margin of Qaidam Basin. *J. Palaeogeogr.*, 2006, **8**(2), 165–173. https://doi.org/10.3969/j.issn.1671-1505.2006.02.003
44. Fu, J. H., Li, S. X., Xu, L. M., Niu, X. B. Paleo-sedimentary environmental restoration and its significance of Chang 7 Member of Triassic Yanchang Formation in Ordos Basin, NW China. *Petrol. Explor. Dev.*, 2018, **45**(6), 998–1008. https://doi.org/10.1016/S1876-3804(18)30104-6
45. Lei, B. J., Que, H. P., Hu, N., Niu, Z. J., Wang, H. Geochemistry and sedimentary environments of the Palaeozoic siliceous rocks in western Hubei. *Sediment. Geol. Tethyan Geol.*, 2002, **22**(2), 70–79.
46. Li, L., Liu, Z. J., George, S. C., Sun, P. C., Xu, Y. B., Meng, Q. T., Wang, K. B., Wang, J. X. Lake evolution and its influence on the formation of oil shales in the Middle Jurassic Shimengou Formation in the Tuanyushan area, Qaidam Basin, NW China. *Geochem.*, 2019, **79**(1), 162–177. https://doi.org/10.1016/j.geoch.2018.12.006
47. Wignall, P. B., Twitchett, R. J. Oceanic anoxia and the end Permian mass extinction. *Science*, 1996, **272**(5265), 1155–1158. https://doi.org/10.1126/science.272.5265.1155
48. Hallberg, R. O. A. Geochemical method for investigation of pale-oredox conditions in sediments. *Ambio Spec. Rep.*, 1976, **4**, 139–147.
49. Acharya, S. S., Panigrahi, M. K., Gupta, A. K., Tripathy, S. Response of trace

metal redox proxies in continental shelf environment: the Eastern Arabian Sea scenario. *Cont. Shelf Res.*, 2015, **106**, 70–84. https://doi.org/10.1016/j.csr.2015.07.008

50. Tribovillard, N., Algeo, T. J., Lyons, T., Riboulleau, A. Trace metals as paleoredox and paleoproductivity proxies: an update. *Chem. Geol.*, 2006, **232**(1–2), 12–32. https://doi.org/10.1016/j.chemgeo.2006.02.012
51. McLennan, S. M. Weathering and global denudation. *J. Geol.*, 1993, **101**(2), 295–303. https://doi.org/10.1086/648222
52. Fedo, C. M., Nesbitt, H. W., Young, G. M. Unraveling the effects of potassium metasomatism in sedimentary rocks and paleosols, with implications for paleoweathering conditions and provenance. *Geology*, 1995, **23**(10), 921–924. https://doi.org/10.1130/0091-7613(1995)023%3C0921:UTEOPM%3E2.3.CO;2
53. McLennan, S. M., Taylor, S. R. Sedimentary rocks and crustal evolution: tectonic setting and secular trends. *J. Geol.*, 1991, **99**(1), 1–21. https://doi.org/10.1086/629470
54. Liu, R., Liu, Z. J., Sun, P. C., Xu, Y. B., Liu, D. Q., Yang, X. H., Zhang, C. Geochemistry of the Eocene Jijuntun Formation oil shale in the Fushun Basin, northeast China: implications for source-area weathering, provenance and tectonic setting. *Geochem.*, 2015, **75**(1), 105–116. https://doi.org/10.1016/j.chemer.2014.08.004
55. Song, Y., Liu, Z. J., Meng, Q. T., Wang, Y. M., Zheng, G. D., Xu, Y. B. Petrography and geochemistry characteristics of the lower Cretaceous Muling Formation from the Laoheishan Basin, Northeast China: implications for provenance and tectonic setting. *Mineral. Petrol.*, 2017, **111**(3), 383–397. https://doi.org/10.1007/s00710-016-0476-9
56. Floyd, P. A., Leveridge, B. E. Tectonic environment of the Devonian Gramscatho basin, south Cornwall: framework mode and geochemical evidence from turbiditic sandstones. *J. Geol. Soc.*, 1987, **144**(4), 531–542. https://doi.org/10.1144/gsjgs.144.4.0531
57. Wronkiewicz, D. J., Condie, K. C. Geochemistry of Archean shales from the Witwatersrand Supergroup, South Africa: source-area weathering and provenance. *Geochim. Cosmochim. Acta*, 1987, **51**(9), 2401–2416. https://doi.org/10.1016/0016-7037(87)90293-6
58. Bhatia, M. R., Crook, K. A. W. Trace element characteristics of greywackes and tectonic setting discrimination of sedimentary basins. *Contrib. Mineral. Petrol.*, 1986, **92**(2), 181–193. http://dx.doi.org/10.1007/BF00375292
59. Maynard, J. B., Valloni, R., Yu, H. S. Composition of modern deep-sea sands from arc-related basins. *Geol. Soc. Lond. Spec. Publ.*, 1982, **10**(1), 551–561. https://doi.org/10.1144/GSL.SP.1982.010.01.36
60. Bhatia, M. R. Plate tectonics and geochemical composition of sandstone. *J. Geol.*, 1983, **91**(6), 611–627. http://dx.doi.org/10.1086/628815
61. Armstrong-Altrin, J. S., Verma, S. P. Critical evaluation of six tectonic setting discrimination diagrams using geochemical data of Neogene sediments from known tectonic settings. *Sediment. Geol.*, 2005, **177**(1–2), 115–129. https://doi.org/10.1016/j.sedgeo.2005.02.004

62. Ma, P. F., Wang, L. C., Wang, C. S., Wu, X. H., Wei, Y. S. Organic-matter accumulation of the lacustrine Lunpola oil shale, central Tibetan Plateau: controlled by the paleoclimate, provenance, and drainage system. *Int. J. Coal Geol.*, 2015, **147–148**, 58–70. https://doi.org/10.1016/j.coal.2015.06.011
63. He, Z. H., Liu, Z. J., Guo, W. The heavy mineral analysis and its geological significance of Dameigou section in northern Qaidam Basin. *World Geol.*, 2001, **20**(3), 279–284, 312.
64. Wang, T., Liu, Z. J., Sun, P. C., Bai, Y. Y., Song, S. Sandstone detrital composition and provenance tectonic attributes of Middle Jurassic Shimengou Formation in Yuqia area of Qaidam Basin. *Global Geol.*, 2018, **38**(1), 154–161.
65. Feng, H. W., Xu, S. M., Wang, J. D., Zhang, G. L., Zeng, Z. P., Shu, P. C. Jurassic provenances and their transition mechanism of the Delingha Sag in the eastern segment of northern margin of the Qaidam Basin, North Tibet. *Geosyst. Geoenviron*., 2022, **1**(4), 100097. https://doi.org/10.1016/j.geogeo.2022.100097
66. Yu, L., Xiao, A. C., Wu, L., Tian, Y. T., Rittner, M., Lou, Q. Q., Pan, X. T. Provenance evolution of the Jurassic northern Qaidam Basin (West China) and its geological implications: evidence from detrital zircon geochronology. *Int. J. Earth Sci.*, 2017, **106**, 2713–2726. https://ui.adsabs.harvard.edu/link_gateway/2017IJEaS.106.2713Y/doi:10.1007/s00531-017-1455-z
67. Qian, T., Wang, Z. X., Wang, Y., Liu, S. F., Gao, W. L., Li, W. P. Jurassic evolution of the Qaidam Basin in western China: constrained by stratigraphic succession, detrital zircon U–Pb geochronology and Hf isotope analysis. *Geol. Soc. Am. Bull.*, 2021, **133**(11–12), 2291–2318.
68. Qinghai Bureau of Geology and Mineral Resources. *Regional Geology of Qinghai Province*. Geological Publishing House, Beijing, 1991.
69. Hu, Q. T., Guan, P., Wang, D. H., Li, S. E., Xiao, Y. J., Zhang, C., Bai, L., Zhang, J. H. Provenance analysis of the Middle Jurassic in northeastern Qaidam Basin: evidence from heavy minerals, elemental geochemistry and detrital zircon U–Pb geochronology. *Acta Sedimentol. Sin.*, 2024, **42**(2), 466-485. https://doi.org/10.14027/j.issn.1000-0550.2022.044
70. Li, H. R. *Research on Metallogenesis of Polymetal Deposits in the Phanerozoic Continental Volcanic Rocks Areas, the Periphery of Qaidam Block, Qinghai Province*. PhD thesis. Jilin University, Changchun, 2021.
71. Cheng, Y. Z., Gao, R., Lu, Z. W., Li, W. H., Wang, G. W., Chen, S., Wu, G. W., Cai, Y. G. Deep structure and dynamics of the eastern segment of the Qilian orogenic belt in the northeastern margin of the Tibetan Plateau. *Earth Sci. Fronti.*, 2023, **30**(5), 314–333.
72. Sun, J. P., Chen, S. Y., Liu, C. L., Ma, Y. S., Yin, C. M., Peng, Y., Shao, P. C., Ma, S., Liu, J. Tectonic setting of northeastern Qaidam Basin and its evolution during the Late Paleozoic: evidence from geochemical characteristics of detrital rock. *Earth Sci. Front.*, 2016, **23**(5), 45–55. https://doi.org/10.13745/j.esf.2016.05.005
73. Hou, H. H., Liu, S. J., Shao, L. Y., Li, Y. H., Zhao, M. E., Cui, W. Elemental geochemistry of the Middle Jurassic shales in the northern Qaidam Basin,

northwestern China: constraints for tectonics and paleoclimate. *Open Geosci.*, 2021, **13**(1), 1448–1462. https://doi.org/10.1515/geo-2020-0318

74. Hu, S. Q., Guo, W. P., Cao, Y. J., Huang, J. X., Mou, Z. H. Tectonic framework and structure evolution of Mesozoic and Cenozoic in the northern margin of Qaidam Basin. *Xinjiang Pet. Geol.*, 2001, **22**(1), 13–16.